scientific reports

Check for updates

OPEN

Efficacy of glutathione inhibitor eprenetapopt against the vulnerability of glutathione metabolism in SMARCA4-, SMARCB1- and PBRM1-deficient cancer cells

Mariko Sasaki & Hideaki Ogiwara✉

Mutation of genes related to the SWI/SNF chromatin remodeling complex is detected in 20% of all cancers. The SWI/SNF chromatin remodeling complex comprises about 15 subunits and is classified into three subcomplexes: cBAF, PBAF, and ncBAF. Previously, we showed that ovarian clear cell carcinoma cells deficient in ARID1A, a subunit of the cBAF complex, are synthetic lethal with several genes required for glutathione (GSH) synthesis and are therefore sensitive to the GSH inhibitor eprenetapopt (APR-246). However, we do not know whether cancer cells deficient in SWI/SNF components other than ARID1A are selectively sensitive to treatment with eprenetapopt. Here, we show that SMARCA4-, SMARCB1-, and PBRM1-deficient cells are more sensitive to eprenetapopt than SWI/SNF-proficient cells. We found that deficiency of SMARCA4, SMARCB1, or PBRM1 attenuates transcription of the *SLC7A11* gene (which supplies cysteine as a raw metabolic material for GSH synthesis) by the failure of recruitment of cBAF and PBAF to the promotor and enhancer regions of the *SLC7A11* locus, thereby reducing basal levels of GSH. In addition, eprenetapopt decreased the amount of intracellular GSH and increased the intracellular amount of reactive oxygen species (ROS), followed by induction of apoptosis. Taken together, eprenetapopt could be a promising selective agent for SWI/SNF-deficient cancer cells derived from SMARCA4-deficient lung cancers, SMARCB1-deficient rhabdoid tumors, and PBRM1-deficient kidney cancers.

Mutation of genes encoding components of the SWI/SNF (SWItch/Sucrose Non-Fermentable) chromatin remodeling complex is detected in approximately 20% of all patients with cancer[1,2]. The SWI/SNF chromatin remodeling complex comprises about 15 subunits, and is classified into three complexes: the BRG1/BRM-associated factor (BAF; canonical BAF; cBAF) complex (which includes SMARCA4, SMARCB1, ARID1A, and DPF2); the polybromo-associated BAF (PBAF) complex (which includes SMARCA4, SMARCB1, PBRM1 and ARID2); and the noncanonical BAF (ncBAF) complex (which includes SMARCA4, and BRD9)[3]. ARID1A is mutated in about 46% of ovarian clear cell carcinomas and in 27% of gastric carcinomas[4–6], whereas SMARCA4 and PBRM1 are mutated in about 10% of non-small lung adenocarcinomas and 40% of renal clear cell carcinomas, respectively[7]. Almost all rhabdoid tumors and epithelioid sarcomas are deficient in SMARCB1[8,9]. Most SWI/SNF-related genes cause loss of function and genetic aberrations in cancer cells; therefore, developing treatments based on synthetic lethality is a promising strategy. The SWI/SNF chromatin remodeling complex regulates cellular functions such as transcription, DNA replication, DNA repair, and chromosomal segregation by opening up the chromatin structure[10]. For example, transcription is regulated by various chromatin-regulating factors and transcription factors that promote gene expression. In general, the SWI/SNF complex promotes gene transcription; therefore, it may go unnoticed that aberrations in the promotor function of the SWI/SNF complex generate vulnerabilities that attenuate transcription.

Antioxidants have been proposed as practical strategies to combat DNA damage mediated by ROS (reactive oxygen species)[11,12]. Cellular ROS levels are determined by the balance between generation and elimination, a

Division of Cancer Therapeutics, National Cancer Center Research Institute, 5-1-1, Tsukiji, Chuo-ku, Tokyo 104-0045, Japan. ✉email: hogiwara@ncc.go.jp

process regulated by antioxidant defense mechanisms[11]. Because high levels of ROS cause cell damage and cell death, targeting these antioxidant defense systems is an attractive therapeutic strategy. Eprenetapopt (APR-246) has been tested in clinical trials involving patients with myelodysplastic syndromes (MDS) and acute myeloid leukemia (AML) (ClinicalTrials.gov identifier: NCT03072043)[13]. Eprenetapopt is converted to the Michael acceptor methylene quinuclidinone (MQ), which inhibits the antioxidant metabolite GSH (glutathione) by reacting with its thiol groups[14]. Covalent binding of MQ reduces GSH levels, thereby shifting the intracellular balance between ROS generation and antioxidation toward an increase in ROS levels. Previously, we proposed a novel therapeutic strategy for ARID1A-deficient ovarian and gastric cancers based on targeting vulnerabilities in GSH metabolism[15,16]. ARID1A deficiency impairs transcription of *SLC7A11*(solute carrier family 7 member 11), which is a component of the xCT cystine transporter complex; this maintains the intracellular cysteine balance required for GSH synthesis, thereby decreasing basal GSH levels[17,18]. This low basal level of GSH in ARID1A-deficient ovarian and gastric cancer cells renders them sensitive to inhibition of GSH metabolism by Eprenetapopt[15,16]. The result is increased ROS production and perturbed antioxidant system homeostasis[15,16]. However, although ARID1A-deficient ovarian cancer cells with low GSH levels are vulnerable to inhibition of GSH metabolism, we do not know whether GSH inhibition is an effective treatment for other types of tumors deficient in SWI/SNF.

Results

SMARCA4-, SMARCB1- and PBRM1-deficient cancer cells are sensitive to a GSH inhibitor

Previously, we found that ARID1A-deficient ovarian clear cell carcinoma and gastric cancer cell lines are sensitive to the GSH inhibitor eprenetapopt (APR-246)[15,16]. ARID1A is a subunit of cBAF[3]. SMARCA4, SMARCB1, and PBRM1 are subunits of cBAF/PBAF/ncBAF, cBAF/PBAF, and PBAF, respectively. To investigate whether cells deficient in a SWI/SNF subunit other than ARID1A are sensitive to GSH inhibition, we first established a cancer cell line panel derived from SWI/SNF-proficient cell lines (HCC44, PC9, H2122, H2228), and from SMARCA4-deficient (H1819, H1703, H522, KP-4)[19,20], SMARCB1-deficient (JMU-RTK-2, G401, G402, HS-ES-1), or PBRM1-deficient (RCC-MF, KMRC-1) cell lines (Fig. 1a). We then calculated the IC_{50} (50% inhibitory concentration) values derived from SWI/SNF-proficient cell lines and SMARCA4-, SMARCB1- and PBRM1-deficient cell lines treated with eprenetapopt (Fig. 1b). The IC_{50}values for SMARCA4-, SMARCB1-, and PBRM1-deficient cell lines, as well as ARID1A-deficient cell lines (OVISE and TOV21G)[15], were significantly lower than those for SWI/SNF-proficient cell lines (Fig. 1b). In addition, a drug sensitivity test to eprenetapopt was performed in a rescue cell line (+SMARCB1) in which a SMARCB1 expression vector was introduced against the SMARCB1-deficient cell line JMU-RTK-2 (-SMARCB1) (**Supplementary Fig. 1a**). We found that the IC_{50} value for SMARCB1 rescue cell line (+SMARCB1) treated with eprenetapopt was significantly lower than that for the parent cell line (-SMARCB1) (**Supplementary Fig. 1b**); that is, the SMARCB1 rescue cell line (+SMARCB1) was found to be resistant to eprenetapopt. Thus, it was suggested that the SMARCB1 deficiency contributed to the eprenetapopt sensitivity to SMARCB1-deficient cell lines. Together, these results indicate that eprenetapopt is a promising therapeutic agent for all SMARCA4-, SMARCB1- and PBRM1-deficient cancers in addition to ARID1A-deficient cancers.

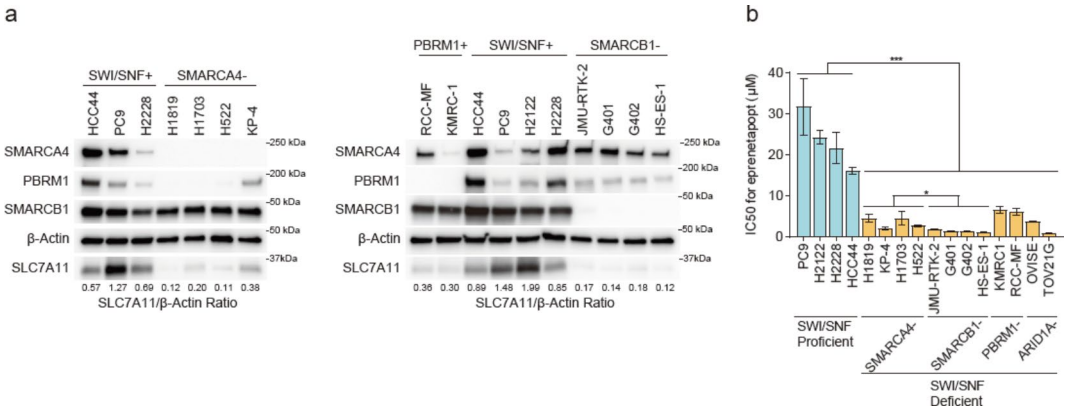

Fig. 1. SWI/SNF-deficient cancer cells are sensitive to GSH inhibition. (**a**). Immunoblot analysis of SMARCA4, SMARCB1, PBRM1, SLC7A11, and β-actin expression in a cancer cell line panel. The ratio of the signal intensity of SLC7A11 protein relative to that of β-actin protein was calculated. (**b**). IC_{50} values for eprenetapopt (APR-246) in cancer cell lines derived from SWI/SNF-proficient cell lines (PC9, H2122, H2228, HCC44) and SMARCA4-deficient (H1819, KP-4, H1703, H522), SMARCB1-deficient (JMU-RTK-2, G401, G402, HS-ES-1), or PBRM1-deficient (KMRC-1, RCC-MF) cell lines after treatment for 6 days. Data are presented as the mean ± SEM (standard error of the mean), $n = 3$ independent experiments. p values were determined by an unpaired two-tailed Student's t-test. $^{*}p < 0.05$, $^{***}p < 0.001$.

SMARCA4-, SMARCB1- and PBRM1-deficient cancer cells have low basal levels of GSH due to attenuated expression of *SLC7A11*

Previously, we showed that ARID1A deficiency attenuated transcriptional expression of *SLC7A11*, leading to low basal levels of GSH. Next, we investigated expression of *SLC7A11* mRNA in SMARCA4-, SMARCB1-, and PBRM1-deficient cell lines and found that levels of SLC7A11 protein (Fig. 1a), as well as *SLC7A11* mRNA (Fig. 2a), in SMARCA4-, SMARCB1-, and PBRM1-deficient cell lines were lower than those in SWI/SNF-proficient cell lines.

It has been observed that protein expression of other subunits of cBAF is reduced in the absence of SMARCB1[21,22]. Then, we confirmed the protein expression of a SMARCB1-containing cBAF subunit ARID1A in SMARCB1-proficient HCC44 and H2122 cell lines, and SMARCB1-deficient JMU-RTK-2, G401, G402, and HS-ES-1 cell lines (**Supplementary Fig. 1c**). Expression of SMARCB1 proteins in the SMARCB1-proficient cell lines HCC44 and H2122 was similar, but the expression of the ARID1A protein was higher in HCC44 than in H2122. On the other hand, expression of the ARID1A protein of HS-ES-1 was higher than that of JMU-RTK-2, G401, and G402 in SMARCB1-deficient cell lines. In addition, the expression of the ARID1A protein in SMARCB1-deficient cell lines was not necessarily lower than in SMARCB1-proficient cell lines. The expression level of the ARID1A protein may vary depending on the cell context. Therefore, it was suggested that a deficiency of SMARCB1 reduced the expression of SLC7A11.

Previous studies have assessed the role of SWI/SNF in regulating NRF2-driven targets such as *SLC7A11* and *HMOX1*[23]. They showed that primary human non-small cell lung carcinomas with low levels of SMARCA4 mRNA in the TCGA database do not display differences in expression of not only *SLC7A11* but also *HMOX1*, which are target genes of NRF2 transcription factor[23]. In addition, we showed that primary human renal cell carcinomas with PBRM1 mutation in the TCGA database (**Supplementary Fig. 2a**) and cancer cell lines with mutations of SMARCA4, SMARCB1, ARID1A, and PBRM1 in the CCLE database (**Supplementary Fig. 2b**) did not display differences in expression of *SLC7A11*. However, *SLC7A11*expression in SMARCA4 knockout lung cancer cell lines was lower than in SMARCA4-proficient cells[23]. On the other hand, *HMOX1*expression in SMARCA4 knockout cell lines was higher than that in SMARCA4-proficient cells[23]. These observations suggest that the effect on the expression level of the target gene may be correlated with the presence or absence of SMARCA4 protein expression rather than with the expression level or mutation of the SMARCA4.

SLC7A11 supplies the cell with cystine, which is converted to cysteine before synthesis of GSH[17,18]; therefore, we next examined whether downregulation of SLC7A11 leads to a reduction in GSH synthesis. Basal levels of GSH in SMARCA4-, SMARCB1-, and PBRM1-deficient cell lines were lower than those in SWI/SNF-proficient cell lines (Fig. 2b), suggesting that deficiency of SMARCA4, SMARCB1, and PBRM1 results in downregulation of SLC7A11, followed by a reduction in basal levels of GSH (which is consistent with the findings regarding ARID1A-deficiency)[15,16].

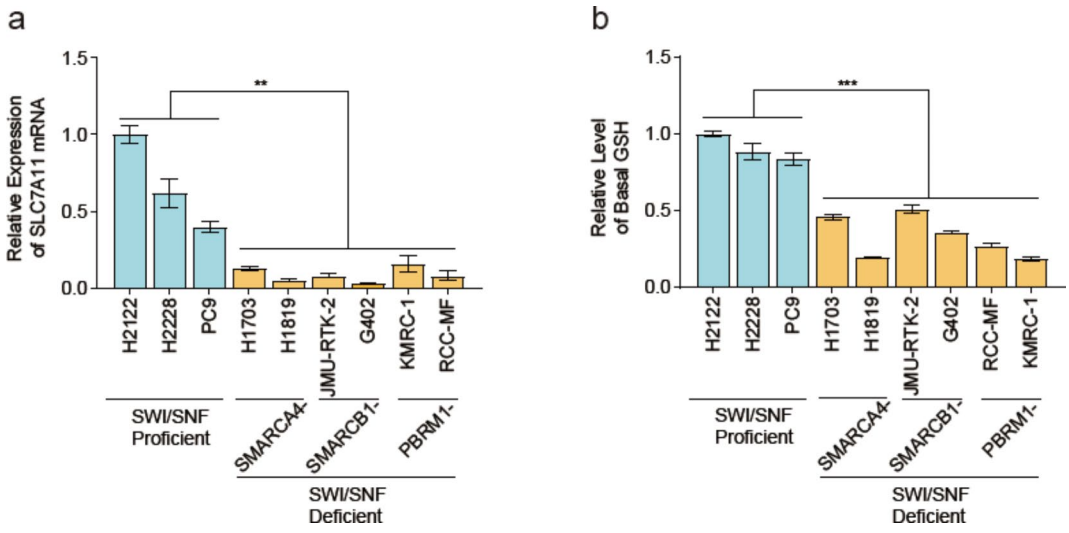

Fig. 2. cBAF- and PBAF-deficient cancer cells show low basal levels of GSH due to attenuated expression of *SLC7A11*. (**a**). Relative expression of *SLC7A11* mRNA in SWI/SNF-proficient cell lines (H2122, H2228, PC9) and SMARCA4-deficient (H1703, H1819), SMARCB1-deficient (JMU-RTK-2, G402), or PBRM1-deficient (KMRC-1, RCC-MF) cell lines (relative to that in the H2122 cell line). Data are presented as SEM (the mean ± standard error of the mean), $n = 3$ independent experiments. (**b**). Basal levels of GSH in SWI/SNF-proficient cell lines (H2122, H2228, PC9) and SMARCA4-deficient (H1703, H1819), SMARCB1-deficient (JMU-RTK-2, G402), or PBRM1-deficient (RCC-MF, KMRC-1) cell lines (relative to that in the H2122 cell line). Data are presented as SEM, $n = 3$ independent experiments. For all experiments, p values were determined by an unpaired two-tailed Student's t-test. $^{**}p < 0.01$, $^{***}p < 0.001$.

Recruitment of cBAF and PBAF complexes is required for transcription of *SLC7A11*

To determine the mechanism underlying the attenuation of *SLC7A11* mRNA expression in SWI/SNF-deficient cancer cells, we investigated the involvement of SMARCA4 (a component of cBAF, PBAF, and ncBAF) and SMARCB1 (a component of cBAF and PBAF) in transcriptional upregulation of *SLC7A11*. We used published ChIP-seq (chromatin immunoprecipitation sequencing) and ATAC-seq (assay for transposase-accessible chromatin with sequencing [which is a marker of open chromatin] (GSE117735 and GSE124903))[24,25] data to investigate whether SMARCA4 and SMARCB1 are recruited directly to the *SLC7A11* locus to regulate transcription. We found that SMARCA4 (a subunit of cBAF, PBAF, and ncBAF) ChIP-seq and ATAC-seq signals in SMARCA4-rescued cells (+SMARCA4) derived from SMARCA4-deficient BIN-67 cell lines localized to proximal and distal regions of the TSS (transcription start site) of the *SLC7A11* gene locus (Fig. 3a). This indicates that SMARCA4 localizes to promoter and enhancer regions. In addition, SMARCA4 ChIP-seq and ATAC-seq signals at regions proximal and distal from the TSS of the *SLC7A11* gene locus in SMARCA4-deficient cells (-SMARCA4) were lower than those in SMARCA4-rescued cells (+SMARCA4) (Fig. 3a). Concordantly, mRNA signals of *SLC7A11* gene were attenuated by SMARCA4 deficiency (Fig. 3a). This indicates that SMARCA4 deficiency reduced open chromatin at the promotor and enhancer regions of the *SLC7A11* locus, thereby attenuating transcription of *SLC7A11*.

On the other hand, the data of SMARCA4 (3 independent experiments) and ATAC-seq (4 independent experiments) were reanalyzed from a public database GSE151026[26] (**Supplementary Fig. 3b**). We were unable to confirm the localization of SMARCA4 in +SMARCA4 cells near the TSS of the *SLC7A11* locus. In addition, there was no significant difference in signal intensity near TSS between +SMARCA4 cells and -SMARCA4 cells for ATAC-seq signaling. We also examined loci (*ANKRD1, CDKN1A*)[24,27], which are reported to be localized in loci other than *SLC7A11*. GSE117735[25] data showed that SMARCA4 was localized near TSS in +SMARCA4 cells at all loci (**Supplementary Fig. 4a and 5a**). In addition, the ATAC-seq signal in +SMARCA4 cells was

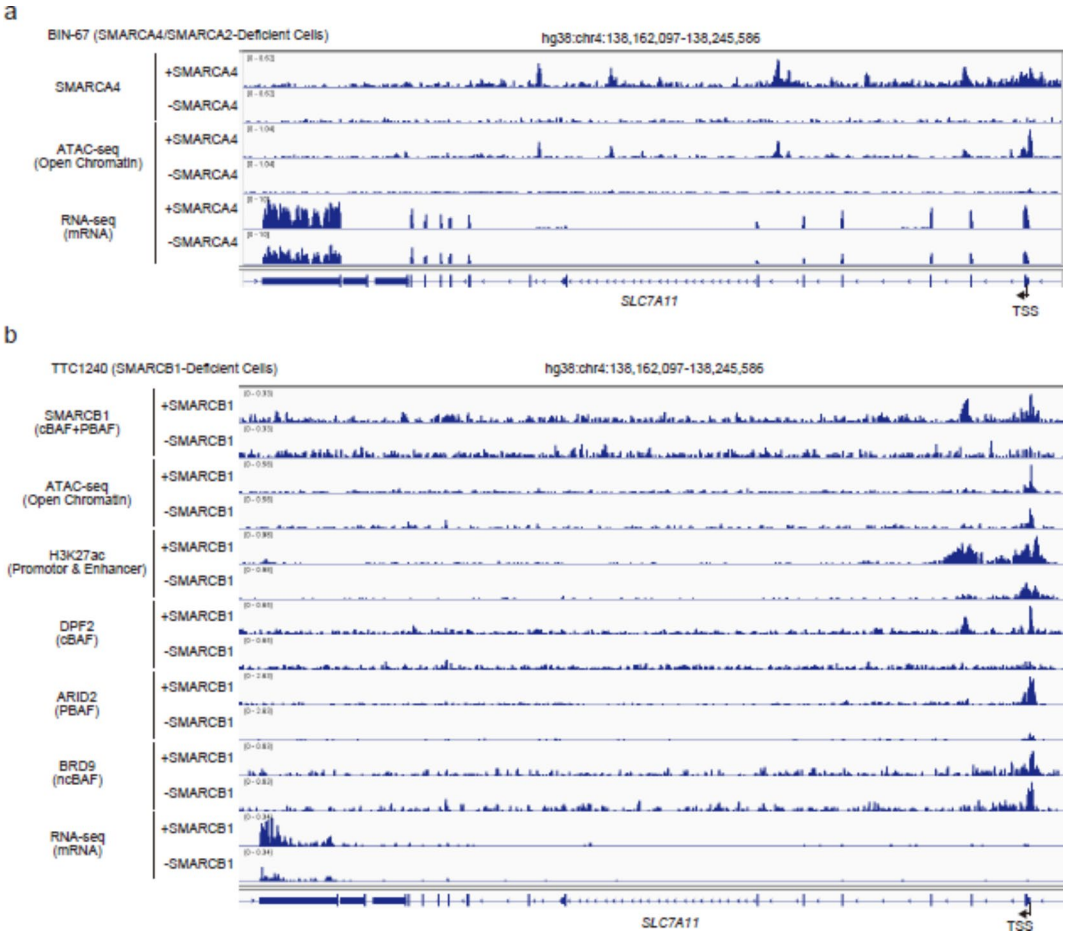

Fig. 3. Recruitment of cBAF and PBAF complexes is required for transcription of *SLC7A11*. (**a**), Localization of signals generated by SMARCA4 ChIP-seq and ATAC-seq around the *SLC7A11* locus in SMARCA4-rescued BIN-67 cells (+SMARCA4) and SMARCA4-deficient BIN-67 (-SMARCA4) cells (derived from published ChIP-seq data and ATAC-seq data; GSE117735). (**b**), Localization of signals generated by SMARCB1, DPF2, ARID2, and H3K27ac ChIP-seq and ATAC-seq around the *SLC7A11* locus in SMARCB1-rescued TTC1240 cells (+SMARCB1) and SMARCB1-deficient TTC1240 cells (-SMARCB1) (derived from published ChIP-seq data and ATAC-seq data; GSE124903).

higher than the ATAC-seq signal in -SMARCA4 cells at the sites proximal or distal from TSS of the *SLC7A11* locus (**Supplementary Fig. 4a and 5a**). On the other hand, GSE151026[26] data showed that no localization of SMARCA4 near TSS was detected in +SMARCA4 cells (**Supplementary Fig. 4b and 5b**). In addition, there was no significant difference in signal intensity between +SMARCA4 cells and -SMARCA4 cells for ATAC-seq signaling at the sites proximal or distal from the TSS site of the *SLC7A11* locus (**Supplementary Fig. 4b and 5b**).

We could not confirm the ChIP-seq results from the Pan et al. report (GSE117735)[25] using similar data from the Orlando et al. result in (GSE151026)[26]. It is speculated that the differences in these data are due to the following differences in experimental conditions. The experimental condition of GSE151026[26] is a transient SMARCA4 transfected cells with a SMARCA4 expression vector for four days. Importantly, reexpression of SMARCA4 in the BIN67 cell line leads to induction of cellular senescence[28] or growth suppression[26]. On the other hand, the experimental conditions of GSE117735 establish a stable cell line of SMARCA4 transfected cells by introducing and further cloning lentiviral vectors expressing SMARCA4. In both sets of experiments, the cells might already undergo senescence when assessed for SMARCA4 binding and open chromatin. One of the differences between both sets of experiments is between the cell conditions four days after gene transfection and the conditions used with stable cell lines due to lentiviral infection. In addition, the Orlando et al. study data came from at least three independent experiments[26], while the Pan et al. study only performed their ChIP-seq study once and the ATAC-seq twice[25]. Another difference is that the Pan et al. data comes from ChIP-seq, and the Orlando et al. data comes from CUT&RUN-seq. Therefore, it is considered that the difference between the two experimental results occurred due to various experimental conditions and differences in experimental methods. However, at least the data from our previous ChIP analysis[15] show that in ARID1A-proficient cells, ARID1A and SMARCA4 are localized to the promoter region of the *SLC7A11* locus, and in ARID1A-knockout cells, their localization is attenuated. Therefore, the localization of SWI/SNF factors in the transcriptional regulatory region of the *SLC7A11* locus may be detected in SWI/SNF-proficient cell lines or cells with long-term stable expression of SWI/SNF factors.

Similarly, SMARCB1 (a subunit of cBAF and PBAF) ChIP-seq signals in SMARCB1-rescued cells (+SMARCB1) derived from SMARCB1-deficient TTC1240 cell lines localized to regions proximal and distal from the TSS of the *SLC7A11* locus (Fig. 3b). In addition, ATAC-seq and H3K27ac (a maker of transcriptional promotion) ChIP-seq signals in SMARCB1-rescued cells (+SMARCB1) localized to the TSS of the *SLC7A11* locus (Fig. 3b). However, SMARCB1 deficiency (-SMARCB1) concordantly reduced the ATAC-seq, H3K27ac signals, and mRNA signals at the TSS site (Fig. 3b). This indicates that SMARCB1 deficiency reduced open chromatin at the promotor and enhancer regions of the *SLC7A11* locus, thereby attenuating transcription of *SLC7A11*. In addition, DPF2 (a subunit of cBAF) in SMARCB1-rescued cells (+SMARCB1) localized to regions proximal and distal from the TSS of the *SLC7A11* locus (Fig. 3b). On the other hand, ARID2 (a subunit of PBAF) in SMARCB1-rescued cells (+SMARCB1) localized only to the region proximal from the TSS of the *SLC7A11* locus (Fig. 3b). BRD9 (a subunit of ncBAF) as well as cBAF (DPF2) and PBAF (ARID2) are also localized to the TSS region of the *SLC7A11* locus (Fig. 3b). Interestingly, the SMARCB1 deficiency reduced the localization of the *SLC7A11* loci of the DPF2 (cBAF) and ARID2 (PBAF) complexes to the TSS region, but did not affect the localization of ncBAF (Fig. 3b). However, knockdown of BRD9 (ncBAF) did not reduce SLC7A11 expression in SMARCB1-deficient cell lines (**Supplemental Fig. 6a-b**). These results suggest that the cooperative relationship of the cBAF and PBAF complexes regulates the transcription of the SLC7A11 gene. Still, the absence of cBAF or PBAF of the complexes attenuates the transcription of *SLC7A11*. These results indicate that the cBAF and PBAF complexes localize to the promotor and enhancer regions of the *SLC7A11* locus to facilitate transcription by opening chromatin cooperatively.

Induction of apoptosis via inhibition of GSH in SMARCA4-, SMARCB1- and PBRM1-deficient cells is caused by a decrease in GSH followed by an increase in ROS

Eprenetapopt inhibits the antioxidant metabolite GSH by reacting with its thiol residues[14]. Covalent binding to GSH reduced the levels of GSH, thereby shifting the intracellular balance of ROS generation/antioxidant responses toward ROS generation. Therefore, we next examined whether eprenetapopt inhibits GSH in SMARCA4-, SMARCB1-, and PBRM1-deficient cell lines. The data showed that eprenetapopt led to a marked reduction in GSH levels in SMARCA4-, SMARCB1-, and PBRM1-deficient cell lines but did not affect GSH levels in SWI/SNF-proficient cell lines (Fig. 4a). By contrast, ROS levels increased more markedly in SMARCA4-, SMARCB1-, and PBRM1-deficient cell lines than in SWI/SNF-proficient cell lines (Fig. 4b). Moreover, eprenetapopt induced apoptosis of SMARCA4-, SMARCB1-, and PBRM1-deficient cell lines, as demonstrated by higher levels of cleaved caspase activation than in SWI/SNF-proficient cell lines (Fig. 4c). To investigate whether increased ROS induces apoptosis, we examined the effect of the combination of the ROS inhibitor NAC (N-Acetyl-L-cysteine) on cleaved caspase 3/7 signaling when treated with eprenetapopt. In the SMARCA4-deficient cell lines H1819 and H1703 and SMARCB1-deficient cell lines JMU-RTK-2 and G402, ROS and cleaved caspase 3/7 signals were increased by treatment with eprenetapopt but suppressed by treatment with NAC (Fig. 4d and e). Therefore, it was indicated that ROS increased by treating eprenetapopt, and the ROS induced apoptosis. These results suggest that increased oxidative stress induced by GSH inhibitors in SMARCA4-, SMARCB1-, and PBRM1-deficient cells also induces cell death.

Discussion

Previously, we showed that ARID1A-deficient cancers are vulnerable to GSH inhibition through attenuated transcription of *SLC7A11*[15,16]. Because ARID1A is a component of the cBAF complex, it is suggested that the cBAF complex is required for transcription of *SLC7A11*. Here, we show that SMARCA4-, SMARCB1- and PBRM1-deficient cell lines show reduced *SLC7A11* expression and high sensitivity to eprenetapopt, indicating that the PBAF complex in addition to the cBAF complex is required for expression of *SLC7A11*. We also showed

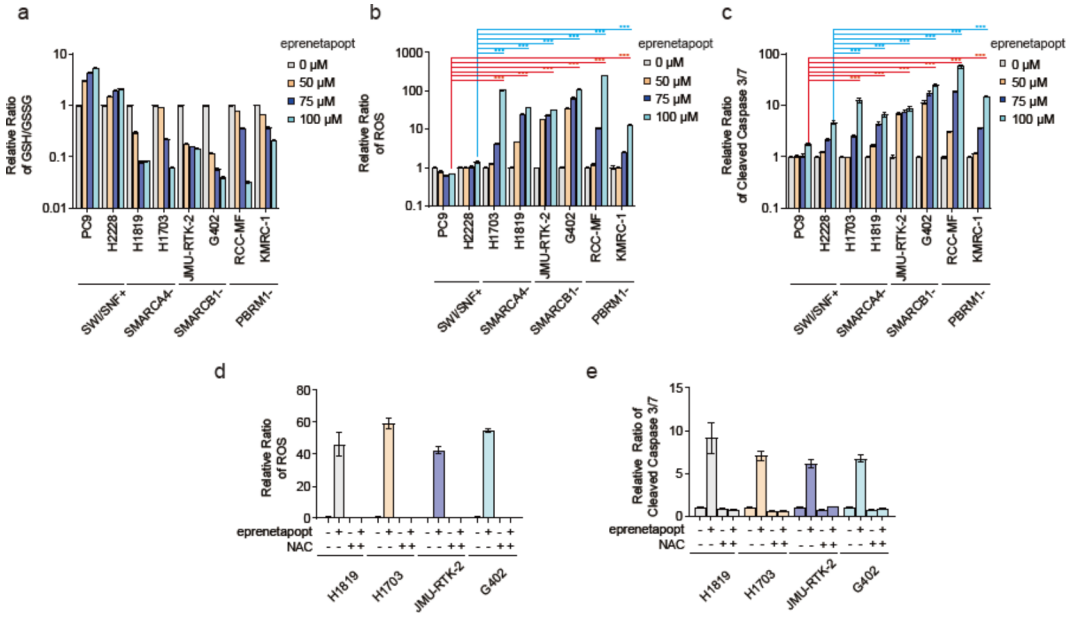

Fig. 4. Apoptosis induced by GSH inhibition in cBAF- and PBAF-deficient cells is due to a decrease in GSH and a concomitant increase in ROS. (**a**). Relative levels of GSH/GSSG (i.e., reduced GSH/oxidized GSH disulfide) in SWI/SNF-proficient cell lines (PC9, H2228) and SMARCA4-deficient (H1819, H1703), SMARCB1-deficient (JMU-RTK-2, G402), or PBRM1-deficient (RCC-MF, KMRC-1) cell lines treated with 0, 50, 75, or 100 μM eprenetapopt (APR-246) for 24 h. Data are presented as the mean ± SD (standard deviation), $n = 3$ independent experiments. (**b**). Relative ROS levels in SWI/SNF-proficient cell lines (PC9, H2228) and SMARCA4-deficient (H1703, H1819), SMARCB1-deficient (JMU-RTK-2, G402), or PBRM1-deficient (RCC-MF, KMRC-1) cell lines treated with 0, 50, 75, or 100 μM eprenetapopt (APR-246) for 24 h. Data are presented as the mean ± SD, $n = 3$ independent experiments. p values were determined by an unpaired two-tailed Student's t-test. $^{***}p < 0.001$. (**c**). Relative signal intensity generated by cleaved caspase 3 and caspase 7 in SWI/SNF-proficient cell lines (PC9, H2228) and SMARCA4-deficient (H1703, H1819), SMARCB1-deficient (JMU-RTK-2, G402), or PBRM1-deficient (RCC-MF, KMRC-1) cell lines treated with 0, 50, 75, or 100 μM eprenetapopt (APR-246) for 24 h. Data are presented as the mean ± SD, $n = 3$ independent experiments. p values were determined by an unpaired two-tailed Student's t-test. $^{***}p < 0.001$. (**d**). Relative ROS levels in SMARCA4-deficient (H1819, H1703), SMARCB1-deficient (JMU-RTK-2, G402) cell lines treated with or without 100 μM eprenetapopt (APR-246) and 5 mM N-acetyl-L-cysteine (NAC) for 24 h. Data are presented as the mean ± SD, $n = 3$ independent experiments. (**e**). Relative signal intensity generated by cleaved caspase 3 and caspase 7 in SMARCA4-deficient (H1819, H1703), SMARCB1-deficient (JMU-RTK-2, G402) cell lines treated with or without 100 μM eprenetapopt (APR-246) and 5 mM N-acetyl-L-cysteine (NAC) for 24 h. Data are presented as the mean ± SD, $n = 3$ independent experiments.

that ncBAF, as well as cBAF and PBAF, are localized to the TSS of the *SLC7A11* locus. SMARCB1 is a component of the cBAF and PBAF complex, and SMARCB1 deficiency reduced the localization of the *SLC7A11* loci of the cBAF and PBAF but not ncBAF. However, suppression of ncBAF did not affect the *SLC7A11* expression. When either SMARCA4, SMARCB1, or PBRM1 is deficient, the transcription of the SLC7A11 may be attenuated by disrupting the coordinated transcriptional regulation between the cBAF and PBAF complexes. Therefore, the absence of cBAF or PBAF of the complexes attenuates the transcription of SLC7A11 (Fig. 5a).

The IC50 value of the SMARCA4-deficient cell line group tended to be significantly higher than the IC50 value of the SMARCB1-deficient cell line group (Fig. 1b). This may be due to differences in the SWI/SNF subcomplex, which affects when SMARCA4 and SMARCB1 are deficient. The results of our study indicate that the cBAF and PBAF subcomplexes are involved in the expression of SLC7A11. SMARCB1 is contained in the cBAF and PBAF subcomplexes, and the absence of SMARCB1 is thought to affect the function of the cBAF and PBAF complexes. On the other hand, since the cBAF complex and the PBAF complex contain SMARCA4 and SMARCA2 mutually exclusively, the absence of SMARCA4 does not affect the function of the cBAF subcomplex and the PBAF complex, including SMARCA2. It is conceivable that SMARCB1 deficiency showed a high sensitivity to Eprenetapopt to involve the entire cBAF and PBAF complexes. On the other hand, SMARCA4 deficiency may have affected only a portion of the cBAF and PBAF complexes (i.e., the function of the cBAF and PBAF complexes, including SMARCA2, remains). Thus, the sensitivity of Eprenetapopt in SMARCA4-deficient cell lines may have been weaker than in SMARCB1-deficient cell lines.

Together with previous data[15], the data presented herein suggest a mechanism by which SWI/SNF chromatin remodeling complexes are involved in the transcriptional regulation of *SLC7A11* (Fig. 5b, c). cBAF localizes to the promotor and enhancer regions of the *SLC7A11* locus, whereas PBAF and ncBAF localizes only to the promotor regions of the *SLC7A11* locus. The cBAF, PBAF and ncBAF complexes act cooperatively to remodel chromatin

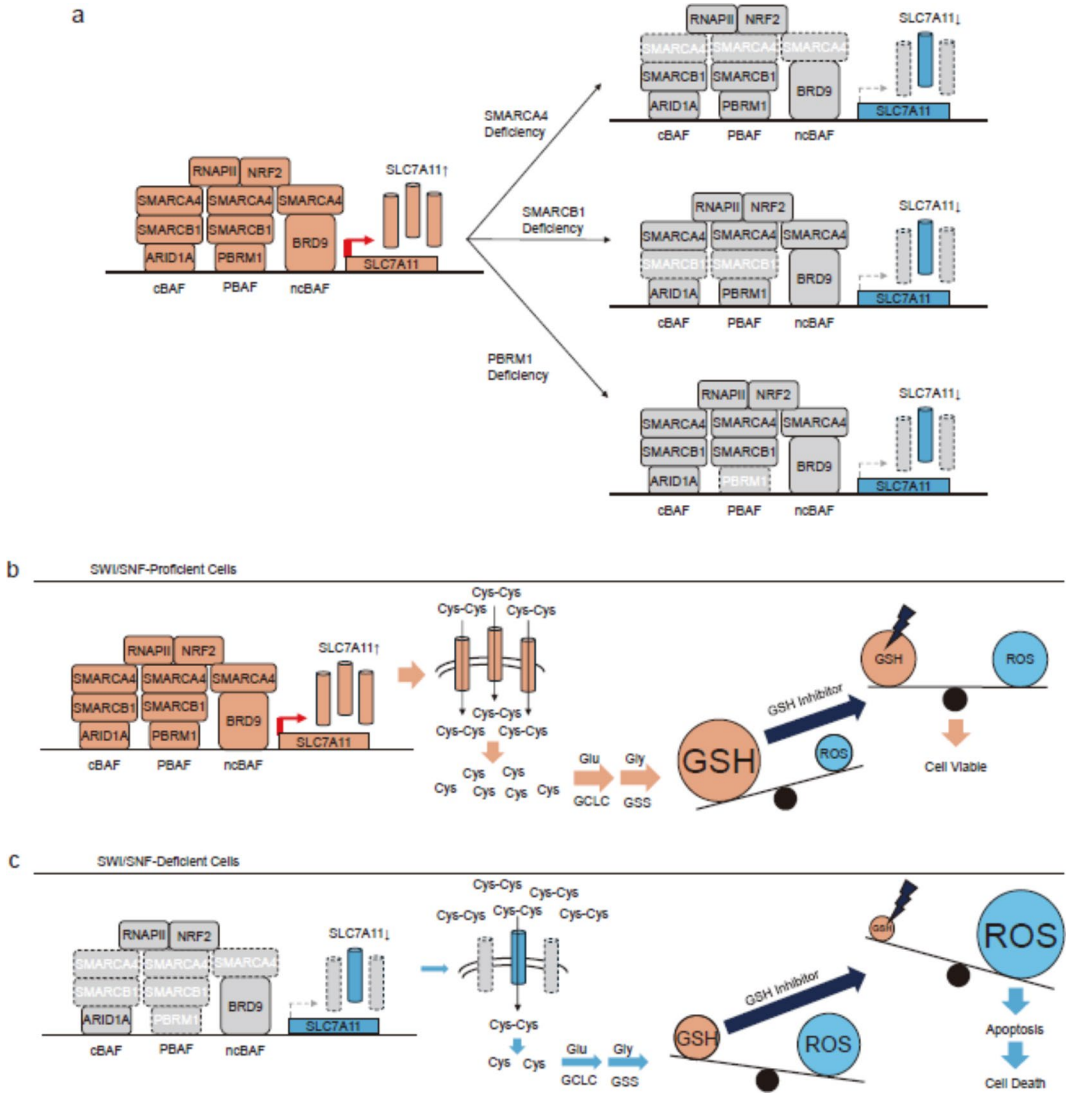

Fig. 5. A schematic model of the mechanism underlying transcriptional regulation of SLC7A11 expression by SWI/SNF chromatin remodeling complexes. (**a**). A Schematic model of transcriptional regulation of the *SLC7A11* gene in cooperation with cBAF, PBAF, and ncBAF complexes. cBAF (SMARCA4, ARID1A, SMARCB1) localizes to the promotor and enhancer regions of the *SLC7A11* locus. PBAF (SMARCA4, PBRM1, SMARCB1) and ncBAF (SMARCA4, BRD9) localize to the promotor region of the *SLC7A11* locus. When either SMARCA4, SMARCB1, or PBRM1 is deficient, the transcription of the SLC7A11 is attenuated by disrupting the coordinated transcriptional regulation among the cBAF, PBAF, and ncBAF complexes. Therefore, the absence of any of the complexes attenuates the transcription of SLC7A11. (**b**). A Schematic model of transcriptional regulation of the *SLC7A11* gene and the balance between GSH and ROS in SWI/SNF-proficient cells. The BAF, PBAF, and ncBAF complexes act cooperatively to remodel the chromatin at the promotor and enhancer regions of the *SLC7A11* locus, thereby facilitating transcription. This is followed by recruiting transcription factors such as NRF2 and RNA polymerases II (RNAPII). SLC7A11 incorporates Cystine (Cys-Cys) into the cells, and then Cys is produced in cells. Cys (cysteine) is associated with Glu (glutamate) and Gly (glycine), and Glutathione (GSH) is made in excess of the amount of ROS in the cell. At this time, even if a GSH inhibitor is administered, ROS can be suppressed, so the cell survives. (**c**). A Schematic model of transcriptional regulation of the *SLC7A11* gene and the balance between GSH and ROS in SWI/SNF-deficient cells. Deficiency in either cBAF or PBAF suppresses the recruitment of transcription factors, leading to repressed expression of *SLC7A11*. This reduces cystine uptake, resulting in a shortage of intracellular cysteine. Because Glutathione (GSH) is synthesized from Cystine (Cys-Cys), Glu (glutamate), and Gly (glycine), a shortage of Cys (cysteine) leads to a reduction in GSH synthesis. Thus, SMARCA4-, SMARCB1- and PBRM1-deficient cells have low levels of GSH, making them vulnerable to ROS. Further suppressing GSH in SMARCA4-, SMARCB1- and PBRM1-deficient cells by treatment with eprenetapopt decreases basal levels of GSH to an even greater extent. This ultimately leads to an increase in intracellular ROS, which triggers apoptosis-mediated cell death.

at the promotor and enhancer regions of the *SLC7A11* locus to facilitate transcription, which is followed by recruitment of transcription factors such as NRF2 (anti-oxidant regulator) and RNAPII (RNA polymerases II)[15,16] (Fig. 5b). However, deficiency in either SMARCA4, SMARCB1 or PBRM1 attenuates recruitment of these transcription factors, thereby repressing expression of *SLC7A11*, which then reduces transport of cystine into cells; the ultimate result is a shortage of intracellular cysteine (Fig. 5c). Because GSH is synthesized from cysteine, glycine, and glutamate, a shortage of cysteine reduces synthesis of GSH (Fig. 5c). Thus, cells deficient in SMARCA4, SMARCB1 or PBRM1 have low levels of GSH, making the cells vulnerable to ROS (Fig. 5c). Therefore, inhibiting GSH in SWI/SNF-deficient cancer cells using eprenetapopt (APR-246) deals another blow by further decreasing basal GSH levels, thereby increasing basal ROS levels, which trigger apoptosis (Fig. 5c).

In lung cancer cell line models, the *HMOX1* gene has increased SMARCA4 suppression of NRF2 binding to transcriptional regulatory regions and increased gene expression[23]. Contrary to this phenomenon, in colorectal cancer cell line models, the *HMOX1* gene has SMARCA4 suppression that reduces NRF2 binding to transcriptional regulatory regions and reduces gene expression[29]. These contradictory phenomena may be due to differences in the regulatory mechanisms of the SWI/SNF complex and NRF2 in the oxidative stress response, depending on the environment of the organ or cell. However, the expression of NRF2 target genes appears to be correlated with the binding of NRF2 to transcriptional regulatory regions. Therefore, in this study, the attenuation of *SLC7A11* expression in SWI/SNF-deficient cell lines suggests that the binding of NRF2 to transcriptional regulation is attenuated by SWI/SNF deficiency.

SWI/SNF-proficient H2228 cells have an *NFE2L2G31A* activating mutation of *NRF2* gene (*NFE2L2*)[30]. On the other hand, SWI/SNF-proficient H2122 cells have KEAP1 mutation (A170_R204del), which leads to activation of NRF2[30]. In addition, H2122 cells have STK11 mutations (P281RfsTer6) and KRAS mutations (G12C), which are highly correlated with increased expression of NRF2 target gene[30]. In addition, SWI/SNF-proficient PC9 and HCC44 cells did not have the above genetic abnormalities. Because the expression of SLC7A11 proteins in H2122 cells is higher than in other SWI/SNF proficient cell lines, high expression levels of SLC7A11 in H2122 cells may be associated with genetic abnormalities involved in multiple NRF2 activations. However, despite the presence of NRF2 activating mutations in H2228, SLC7A11 expression in H2228 cells was lower than in PC9 cells and comparable to that of HCC44 cells. Although it is conceivable that PC9 and HCC44 may also have some abnormalities that activate NRF2, it may suggest that the presence of proficient SWI/SNF complexes contributes to the expression of SLC7A11 rather than that NRF2 activating mutations are involved in high expression of SLC7A11.

Eprenetapopt (APR-246) is a first-in-class small molecule compound that selectively induces apoptosis in *TP53*-mutant cancer cells. Eprenetapopt (APR-246) is a prodrug converted to MQ, which binds covalently to cysteine residues in mutant p53, leading to changes in the functional conformation of the p53 protein[31]. In addition, eprenetapopt (APR-246) increases ROS levels by depleting GSH[32]. Eprenetapopt (APR-246) acts synergistically with azacitidine when used to treat *TP53*-mutant MDS and AML[13,33]. Mutations in *ARID1A* and *TP53* tend to be mutually exclusive in ovarian clear cell carcinomas[1]. Previously, we showed that the sensitivity of ARID1A-deficient cells to eprenetapopt (APR-246) is independent of *TP53* status[15]. Mutation of genes encoding components of the SWI/SNF complex is detected in approximately 20% of all patients with cancer[1,2]. SMARCA4, SMARCB1, and PBRM1 are frequently mutated in 10% of patients with non-small lung adenocarcinomas[7], and in almost patients with rhabdoid tumors, epithelioid sarcomas[8,9], or in 40% of renal clear cell carcinomas[7]. Taken together, the data presented herein suggest that SWI/SNF-deficient cancer cell lines derived from SMARCA4-, SMARCB1-, or PBRM1-deficient cancers are highly sensitive to eprenetapopt (APR-246). Thus, the therapeutic targets of eprenetapopt (APR-246) can be expanded to include SWI/SNF-deficient cancers.

Methods

Materials

Cells were maintained at 37 °C in a humidified incubator containing 5% CO_2. The culture medium comprised DMEM/F-12 (Wako, 048–29785) supplemented with 10% fetal bovine serum (FBS; Gibco/Life Technologies), 10% GlutaMAX Supplement (Gibco, 41550021), 100 U/mL penicillin, and 100 µg/mL streptomycin (Wako, 168–23191). H2228, H2122, H1703, H1819, H522, and TOV21G cells were obtained from the American Type Culture Collection (ATCC). G-401, G-402, KMRC-1, OVISE, KP-4, and JMU-RTK-2 cells were obtained from the Japanese Collection of Research Bioresources (JCRB) Cell Bank. PC9 and HS-ES-1 cells were obtained from the Riken Cell Bank (RCB). RCC-MF was obtained from Cell Lines Service GmbH. HCC-44 was obtained from DSMZ. All cell lines were used for functional experiments after less than 2 months of passage post-receipt. All cell lines tested negative for mycoplasma by MycoAlert (Lonza, LT07-318). Eprenetapopt (APR-246) (Cat# 9000487) and N-acetyl-L-Cysteine (NAC) (Cat# 20261) were purchased from Cayman.

Generation of lentiviruses and virus-infected cells

The cDNA-expressing lentiviral vectors (pLOC-CMV-SMARCB1-Bsd; OHS5897-202619211; Dharmacon) and packaging plasmids (psPAX2: #12260 and pMD2.G: #12259; Addgene) were used for constitutive lentiviral expression of cDNAs. To generate viruses, 293LTV cells were transfected with lentiviral plasmids and packaging plasmids using Lipofectamine 3000 (ThermoFisher Scientific; L3000015). After 16–24 h, the medium was replaced with a fresh growth medium, and cells were incubated for 48 h. Lentivirus-containing supernatants were harvested and concentrated by centrifugation using Lenti-X Concentrator (Takara, 631232). To establish cells infected with viral constructs, cells were transduced with lentivirus suspension containing 8 µg/mL polybrene (Nacalai Tesque, 12996-81) and then incubated for 24 h. The growth medium was then replaced with a fresh medium. After 24–48 h, the cells were incubated for 3–7 days in a growth medium containing 20 µg/mL blasticidin (Wako, 029–18701). To establish JMU-RTK-2 + SMARCB1 cells, SMARCB1-deficient JMU-RTK-2

cells were transduced with lentiviruses derived from the pLOC-CMV-SMARCB1-Bsd lentivirus vector. After selecting blasticidin-resistant cells, a clone of JMU-RTK-2 cells expressing the SMARCB1 protein was isolated.

Immunoblot analysis

To extract proteins, 5×10^5cells were harvested, washed with PBS, and lysed with 150 µL of 1x SDS sample buffer at 95 °C for 5 min. Chromatin was sonicated on ice (20 cycles of 15-second pulses; high setting; 15 s between pulses) using a Bioruptor (M&S Instruments). The cell lysates were quantified using Pierce 660 nm Protein Assay Reagent (Thermo Fisher Scientific, 22660) and Ionic Detergent Compatibility Reagent for Pierce™ 660 nm Protein Assay Reagent (Thermo Fisher Scientific, 22663). Next, 15 µg of protein was analyzed by immunoblotting. SDS-PAGE separated proteins, transferred them to PVDF membranes, and immunoblotted with the indicated antibodies. β-actin was used as a loading control. Membranes were blocked for 1 h at 25 °C with PVDF Blocking Reagent for Can Get Signal (TOYOBO, NYPBR01) and then probed for 1 h at 25 °C with Can Get Signal Solution 1 (TOYOBO, NKB-201) containing primary antibodies. After washing with TBS containing 0.1% Tween 20, the membranes were incubated for 30 min at 25 °C with TBS containing 0.1% Tween 20, 1% BSA, and horseradish peroxidase-conjugated anti-mouse (CST, 7076) or anti-rabbit (CST, 7074) secondary antibodies before visualization using Western Lightning ECL Pro (Perkin Elmer, NEL120001EA). Chemiluminescence signals were measured using a FUSION Chemiluminescence Imaging System (M&S Instruments). Antibodies specific for the following proteins were used for immunoblotting: SMARCA4 (CST, 49360), SMARCB1 (CST, 91735), PBRM1 (CST, 89123), SLC7A11 (CST, 12691), ARID1A (Abcam, ab182560) and β-actin (CST, 4790). Signal intensity was measured using Image J 1.54 g Software[34]. The ratio of the signal intensity of SLC7A11 protein relative to that of β-actin protein was calculated.

Cell viability assay

To measure cell viability after treatment with the inhibitor, cells were trypsinized, counted, and reseeded in 96-well plates at a density of 500 cells per well. After 24 h, cells were treated with the indicated concentrations of Eprenetapopt (APR-246). After 6 days, cell viability was measured using the CellTiter-Glo Luminescent Cell Viability Assay (Promega, G7571). Luminescence was measured using the Nivo plate reader (PerkinElmer). IC_{50} values were calculated using GraphPad Prism 8 (RRID: SCR_002798).

Quantitation of mRNA

To measure basal mRNA levels, 2×10^4 cells were plated into 96-well plates and incubated for 24 h. To establish siRNA-transfected cells, 2×10^4 cells were plated into 96-well plates, transfected with siRNAs (50 nM) using Lipofectamine RNAiMAX (Thermo Fisher Scientific; 13778150), and incubated for 48 h. Next, mRNA was extracted from all cell lines, and cDNA was synthesized using the SuperPrep II Cell Lysis & RT Kit for qPCR (TOYOBO; SCQ-401). Aliquots of cDNA were subjected to quantitative PCR using the THUNDERBIRD Probe qPCR Mix (TOYOBO; QPS101) and TaqMan Gene Expression Assays (Thermo Fisher Scientific). The following gene-specific primer/probe sets were used for SLC7A11 (Hs00921938_m1) and GAPDH (Hs99999905_m1) (Thermo Fisher Scientific). PCR was performed in an ABI StepOnePlus Real-Time PCR System (Applied Biosystems) under the following conditions: denaturation at 95 °C for 15 s, followed by annealing and extension at 60 °C for 30 s (40 cycles). For each sample, the mRNA level of target genes was normalized to that of GAPDH. The target/GAPDH ratios were then normalized against those in control samples using the 2-ΔΔCt method.

Detection of GSH, ROS, and cleaved caspase-3/7

GSH/GSSG, GSH, ROS, and apoptosis were detected using the GSH/GSSG-Glo Assay (Promega, V6611), the GSH-Glo Assay (Promega, V6911), the ROS-Glo H_2O_2 Assay (Promega, G8820), and the Caspase-Glo 3/7 Assay (Promega, G8091), respectively. To measure levels of GSH/GSSG, ROS, and apoptosis after treatment with Eprenetapopt (APR-246) and/or N-acetyl-L-cysteine (NAC), cells were trypsinized and counted and then reseeded in 96-well plates at a density of 1×10^4 cells/well before exposure to drugs at the indicated concentrations. After 16–48 h, luminescence was measured using a Nivo plate reader (PerkinElmer). Cell viability was also measured using the CellTiter-Glo Luminescent Cell Viability Assay (Promega, G7571). GSH, ROS, and Caspase-3/7 levels were normalized to cell viability. The GSH/GSSG ratio was calculated as the GSH-GSSG signal divided by the GSSG/2 signal. Signal ratios in treated samples were normalized against those in untreated samples.

Processing of NGS data

ChIP-seq datasets for BIN-67 and TTC1240 were obtained from publicly available NCBI GEO datasets (GSE117735, GSE124903, GSE151026)[24–26]. These downloaded data were analyzed as described for NGS data processing. Raw sequencing data from ChIP-seq and ATAC-seq were trimmed using fastp version 0.12.4[35]and mapped to the human reference genome (hg38) using Bowtie2 version 2.4.5, with parameters -k 1 --no-mixed --no-discordant -X 2000[36]. Before all downstream analyses, duplicate reads were removed using the MarkDuplicates command in picard-tools version 2.26.11 (http://broadinstitute.github.io/picard). From the ChIP-seq, CPM values in the genome tracks were calculated by subtracting those in the input tracks as the background value for each cell. BigWig files were generated using the bamCompare command from deepTools (RRID: SCR_016366) version 3.5.1, with parameters --operation subtract --normalizeUsing CPM --scaleFactorsMethod None --binSize 10 --smoothLength 30[37], and then visualized by the Integrative Genomics Viewer version 2.13.2[38]. Raw sequencing data from RNA-seq were trimmed using trim-galore version 0.6.5-1 and mapped to the hg38 genome using HISAT2 version 2.2.1[39]. TPM values were calculated using Strand NGS ver 4.0 (TOMY). Genes showing significant changes in expression (i.e., $P < 0.05$ and a 2-fold change $|\log2FC| > 1$)

were identified by Strand NGS ver 4.0 (TOMY). For Venn diagram analysis and Wikipathway analysis of RNA-seq data, the log2-fold change values were plotted using Strand NGS ver 4.0 (TOMY). BigWig files were generated using the bamCoverage command from deepTools version 3.5.1, with parameters --normalizeUsing CPM --binSize 10 --smoothLength 30[37], and then visualized by the Integrative Genomics Viewer (IGV) version 2.13.2[38].

Data availability

The data generated in this study are publicly available in Gene Expression Omnibus (GEO) (RRID: SCR_005012); accession GSE117735[25], GSE124903[24]and GSE151026[26]. Mutation, and gene expression datasets were obtained from the Kidney Renal Clear Cell Carcinoma (TCGA, PanCancer Atlas) database and the Cancer Cell Line Encyclopedia (CCLE, Broad, 2019) database and downloaded from the cBioPortal website ([https://www.cbioportal.org/]). These downloaded data were analyzed as follows. Expression levels of the *SLC7A11* gene among tumors or cell lines with different genetic mutation were isolated. Specifically, the genotype of SMARCA4, ARID1A, PBRM1 or SMARCB1 was determined as the number of altered allele(s) with mutations. Expression of the SLC7A11 gene was compared between samples without mutation and samples with mutation.

Received: 17 April 2024; Accepted: 9 December 2024
Published online: 28 December 2024

References

1. Kadoch, C. et al. Proteomic and bioinformatic analysis of mammalian SWI/SNF complexes identifies extensive roles in human malignancy. *Nat. Genet.* **45**, 592–601. https://doi.org/10.1038/ng.2628 (2013).
2. Kadoch, C. & Crabtree, G. R. Mammalian SWI/SNF chromatin remodeling complexes and cancer: mechanistic insights gained from human genomics. *Sci. Adv.* **1**, e1500447. https://doi.org/10.1126/sciadv.1500447 (2015).
3. Mashtalir, N. et al. Modular Organization and Assembly of SWI/SNF Family Chromatin Remodeling Complexes. *Cell* 175, 1272–1288 e1220, doi: (2018). https://doi.org/10.1016/j.cell.2018.09.032
4. Wiegand, K. C. et al. ARID1A mutations in endometriosis-associated ovarian carcinomas. *N Engl. J. Med.* **363**, 1532–1543. https://doi.org/10.1056/NEJMoa1008433 (2010).
5. Jones, S. et al. Frequent mutations of chromatin remodeling gene ARID1A in ovarian clear cell carcinoma. *Science* **330**, 228–231. https://doi.org/10.1126/science.1196333 (2010).
6. Wang, K. et al. Exome sequencing identifies frequent mutation of ARID1A in molecular subtypes of gastric cancer. *Nat. Genet.* **43**, 1219–1223. https://doi.org/10.1038/ng.982 (2011).
7. Lawrence, M. S. et al. Discovery and saturation analysis of cancer genes across 21 tumour types. *Nature* **505**, 495–501. https://doi.org/10.1038/nature12912 (2014).
8. Chun, H. E. et al. Genome-wide profiles of extra-cranial malignant rhabdoid tumors reveal heterogeneity and dysregulated developmental pathways. *Cancer Cell.* **29**, 394–406. https://doi.org/10.1016/j.ccell.2016.02.009 (2016).
9. Versteege, I. et al. Truncating mutations of hSNF5/INI1 in aggressive paediatric cancer. *Nature* **394**, 203–206. https://doi.org/10.1038/28212 (1998).
10. Sasaki, M. & Ogiwara, H. Synthetic lethal therapy based on targeting the vulnerability of SWI/SNF chromatin remodeling complex-deficient cancers. *Cancer Sci.* **111**, 774–782. https://doi.org/10.1111/cas.14311 (2020).
11. Gorrini, C., Harris, I. S. & Mak, T. W. Modulation of oxidative stress as an anticancer strategy. *Nat. Rev. Drug Discov.* **12**, 931–947. https://doi.org/10.1038/nrd4002 (2013).
12. Harris, I. S. et al. Glutathione and thioredoxin antioxidant pathways synergize to drive cancer initiation and progression. *Cancer Cell.* **27**, 211–222. https://doi.org/10.1016/j.ccell.2014.11.019 (2015).
13. Sallman, D. A. et al. Eprenetapopt (APR-246) and Azacitidine in TP53-Mutant myelodysplastic syndromes. *J. Clin. Oncol.* **39**, 1584–1594. https://doi.org/10.1200/JCO.20.02341 (2021).
14. Tessoulin, B. et al. PRIMA-1Met induces myeloma cell death independent of p53 by impairing the GSH/ROS balance. *Blood* **124**, 1626–1636. https://doi.org/10.1182/blood-2014-01-548800 (2014).
15. Ogiwara, H. et al. Targeting the Vulnerability of Glutathione Metabolism in ARID1A-Deficient Cancers. *Cancer Cell* 35, 177–190 e178, doi: (2019). https://doi.org/10.1016/j.ccell.2018.12.009
16. Sasaki, M. et al. Efficacy of glutathione inhibitors for the treatment of ARID1A-deficient diffuse-type gastric cancers. *Biochem. Biophys. Res. Commun.* **522**, 342–347. https://doi.org/10.1016/j.bbrc.2019.11.078 (2020).
17. Koppula, P., Zhuang, L. & Gan, B. Cystine transporter SLC7A11/xCT in cancer: ferroptosis, nutrient dependency, and cancer therapy. *Protein Cell.* **12**, 599–620. https://doi.org/10.1007/s13238-020-00789-5 (2021).
18. Lin, W. et al. SLC7A11/xCT in cancer: biological functions and therapeutic implications. *Am. J. Cancer Res.* **10**, 3106–3126 (2020).
19. Oike, T. et al. A synthetic lethality-based strategy to treat cancers harboring a genetic deficiency in the chromatin remodeling factor BRG1. *Cancer Res.* **73**, 5508–5518. https://doi.org/10.1158/0008-5472.CAN-12-4593 (2013).
20. Romero, O. A. et al. The tumour suppressor and chromatin-remodelling factor BRG1 antagonizes Myc activity and promotes cell differentiation in human cancer. *EMBO Mol. Med.* **4**, 603–616. https://doi.org/10.1002/emmm.201200236 (2012).
21. Wei, D. et al. SNF5/INI1 deficiency redefines chromatin remodeling complex composition during tumor development. *Mol. Cancer Res.* **12**, 1574–1585. https://doi.org/10.1158/1541-7786.MCR-14-0005 (2014).
22. Wang, X. et al. SMARCB1-mediated SWI/SNF complex function is essential for enhancer regulation. *Nat. Genet.* **49**, 289–295. https://doi.org/10.1038/ng.3746 (2017).
23. Song, S. et al. Loss of SWI/SNF chromatin remodeling alters NRF2 signaling in Non-small Cell Lung Carcinoma. *Mol. Cancer Res.* **18**, 1777–1788. https://doi.org/10.1158/1541-7786.MCR-20-0082 (2020).
24. Valencia, A. M. et al. Recurrent SMARCB1 Mutations Reveal a Nucleosome Acidic Patch Interaction Site That Potentiates mSWI/SNF Complex Chromatin Remodeling. *Cell* 179, 1342–1356 e1323, doi: (2019). https://doi.org/10.1016/j.cell.2019.10.044
25. Pan, J. et al. The ATPase module of mammalian SWI/SNF family complexes mediates subcomplex identity and catalytic activity-independent genomic targeting. *Nat. Genet.* **51**, 618–626. https://doi.org/10.1038/s41588-019-0363-5 (2019).
26. Orlando, K. A. et al. Re-expression of SMARCA4/BRG1 in small cell carcinoma of ovary, hypercalcemic type (SCCOHT) promotes an epithelial-like gene signature through an AP-1-dependent mechanism. *Elife* **9** https://doi.org/10.7554/eLife.59073 (2020).
27. Nakayama, R. T. et al. SMARCB1 is required for widespread BAF complex-mediated activation of enhancers and bivalent promoters. *Nat. Genet.* **49**, 1613–1623. https://doi.org/10.1038/ng.3958 (2017).
28. Karnezis, A. N. et al. Dual loss of the SWI/SNF complex ATPases SMARCA4/BRG1 and SMARCA2/BRM is highly sensitive and specific for small cell carcinoma of the ovary, hypercalcaemic type. *J. Pathol.* **238**, 389–400. https://doi.org/10.1002/path.4633 (2016).

29. Zhang, J. et al. BRG1 interacts with Nrf2 to selectively mediate HO-1 induction in response to oxidative stress. *Mol. Cell. Biol.* **26**, 7942–7952. https://doi.org/10.1128/MCB.00700-06 (2006).
30. Fahrmann, J. F. et al. Mutational activation of the NRF2 pathway Upregulates Kynureninase resulting in Tumor Immunosuppression and Poor Outcome in Lung Adenocarcinoma. *Cancers (Basel)*. 14. https://doi.org/10.3390/cancers14102543 (2022).
31. Lambert, J. M. et al. PRIMA-1 reactivates mutant p53 by covalent binding to the core domain. *Cancer Cell.* **15**, 376–388. https://doi.org/10.1016/j.ccr.2009.03.003 (2009).
32. Bykov, V. J. et al. Targeting of mutant p53 and the Cellular Redox Balance by APR-246 as a strategy for efficient Cancer therapy. *Front. Oncol.* **6**, 21. https://doi.org/10.3389/fonc.2016.00021 (2016).
33. Maslah, N. et al. Synergistic effects of PRIMA-1(Met) (APR-246) and 5-azacitidine in TP53-mutated myelodysplastic syndromes and acute myeloid leukemia. *Haematologica* **105**, 1539–1551. https://doi.org/10.3324/haematol.2019.218453 (2020).
34. Schneider, C. A., Rasband, W. S. & Eliceiri, K. W. NIH Image to ImageJ: 25 years of image analysis. *Nat. Methods*. **9**, 671–675. https://doi.org/10.1038/nmeth.2089 (2012).
35. Chen, S., Zhou, Y., Chen, Y. & Gu, J. Fastp: an ultra-fast all-in-one FASTQ preprocessor. *Bioinformatics* **34**, i884–i890. https://doi.org/10.1093/bioinformatics/bty560 (2018).
36. Langmead, B. & Salzberg, S. L. Fast gapped-read alignment with Bowtie 2. *Nat. Methods*. **9**, 357–359. https://doi.org/10.1038/nmeth.1923 (2012).
37. Ramirez, F., Dundar, F., Diehl, S., Gruning, B. A. & Manke, T. deepTools: a flexible platform for exploring deep-sequencing data. *Nucleic Acids Res.* **42**, W187–191. https://doi.org/10.1093/nar/gku365 (2014).
38. Robinson, J. T. et al. Integrative genomics viewer. *Nat. Biotechnol.* **29**, 24–26. https://doi.org/10.1038/nbt.1754 (2011).
39. Kim, D., Paggi, J. M., Park, C., Bennett, C. & Salzberg, S. L. Graph-based genome alignment and genotyping with HISAT2 and HISAT-genotype. *Nat. Biotechnol.* **37**, 907–915. https://doi.org/10.1038/s41587-019-0201-4 (2019).

Acknowledgements

We thank Hinako Masuda for technical assistance. This study was supported by an AMED grant (JP19ck0106374), by the National Cancer Center Research and Development Fund (2020-A-6), and by the Ono Pharmaceutical Corporation (C2018-130).

Author contributions

Conceptualization: H.O.; Data curation: M.S., H.O.; Formal analysis: H.O.; Funding acquisition: H.O.; Investigations: M.S., H.O.; Methodology: M.S., H.O.; Project administration: M.S., H.O.; Resources: M.S., H.O.; Supervision: H.O.; Validation: M.S., H.O.; Visualization: M.S., H.O.; Writing – review & editing: M.S., H.O.

Declarations

Competing interests

H.O. received grants from the Ono Pharmaceutical Corporation during the study. M.S. declare no potential conflicts of interest.

Additional information

Supplementary Information The online version contains supplementary material available at https://doi.org/10.1038/s41598-024-82753-5.

Correspondence and requests for materials should be addressed to H.O.

Reprints and permissions information is available at www.nature.com/reprints.

Publisher's note Springer Nature remains neutral with regard to jurisdictional claims in published maps and institutional affiliations.